METHODOLOGY TO QUANTIFY CONTRIBUTION OF VARIOUS FEEDTHROUGH SOURCES IN EPI-SEALED DEVICES

Disha Chugh[1], Hyun-Keun Kwon[2,4], Gabrielle D. Vukasin[3,4], and Saurabh A Chandorkar[1*]*
[1]Centre for Nano Science and Engineering (CeNSE), Indian Institute of Science
[2]Centre Apple, Cupertino, CA 95014
[3]Robert Bosch Research and Technology Center, Sunnyvale, CA 94085f
[4]Departments of Electrical & Mechanical Engineering, Stanford University

ABSTRACT

We introduce a methodology for accurately assessing the relative contribution of various feedthrough sources to the overall feedthrough capacitance ($C_{foverall}$) in a capacitively transduced MEMS device. We illustrate this method using an epi-sealed Double-Ended-Tuning-Fork (DETF) device. We also report a counter intuitive result that suggests that segmented transducing electrodes perform better in terms of signal-to-feedthrough ratio than conventionally advocated fully extended electrodes. Additionally, we demonstrate an innovative technique for feedthrough signal cancellation. This new approach improves our ability to optimize device- & PCB-design for minimizing feedthrough effects in a general MEMS device.

KEYWORDS

Micro-resonators, Feedthrough, PCB, Split electrodes, Extended electrodes, Dummy electrode, Dummy differential actuation.

INTRODUCTION

Capacitive MEMS resonators offer miniaturized solutions for various applications, such as inertial sensors, microfluidics devices, optical applications, pressure measurement devices, and RF devices, to name a few [1] [2]. Despite numerous benefits, electrical sensing of capacitive MEMS suffers from the detrimental effects of feedthrough capacitance present in the system. The presence of feedthrough current in the total sensed current can obscure the motional signal or introduce offsets in measured natural frequencies and the Quality-factors [3]. In addition, feedthrough complicates the oscillator design [4], parameter extraction [5], and can impact device sensitivity, particularly in weakly coupled resonators [6].

Extensive research has been done to mitigate the feedthrough signal in MEMS devices [3] [5] [7] [8] [9] [10] [11]. Various post-processing and in-situ methods have been developed to remove the feedthrough signal from the total signal, both in the frequency domain and the time-domain operational strategies. While post-processing methods primarily leverage mathematical tools to remove the feedthrough signal from the total signal, in-situ methods offer diverse array of approaches to minimize feedthrough signal.

Joshua Lee et al. proposed a post-processing method for extracting MEMS resonator parameters from frequency domain signals when the resonant-to-feedthrough signal ratio is less than $\sqrt{2}$ [5]. When this ratio exceeds $\sqrt{2}$, alternative methods presented in [12] [13] [14] can be used. An ingenious method for time-domain post-processing was proposed by A. Brenes et al. who suggested use of pulsed mode actuation [3]. They demonstrated that the feedthrough distortion in time-domain signal is localized in time and hence can be easily removed in the post-processing. Is it also suggested in [3] that subharmonic pulsed-mode actuation outperforms harmonic pulsed-mode actuation, attributed to the spread of distortion in time, around the actuation pulse.

For in-situ cancellation, P. Rantakari et al. proposed using a dummy resonator in conjunction with a differential amplifier to remove feedthrough signal from the total output signal [7]. This method costs precious real-estate on silicon. S. Bhave et al. showed that differential actuation and sensing can reduce feedthrough capacitance significantly [8]. However, Julien Arcamone et al. discusse situations where fully differential actuation/sensing fails to effectively reduce feedthrough signals, and proposed an alternative approach called balanced actuation/sensing as a solution in such cases, especially for bulk-mode resonators, such as, square plate and wine glass resonators [15]. Additionally, Joshua Lee et al. in [10] demonstrated the application of appropriately chosen external package level capacitance with differential input to negate the feedthrough signal in the total output signal. Cheng-Yen Wu demonstrated the utilization of substrate inductance to cancel out the feedthrough signal in [9]. This method can induce undesired oscillations and requires additional circuitry. Furthermore, J. Giner recommended adopting an in-situ adaptive feedthrough cancellation [16] which also requires additional circuitry.

Despite extensive efforts to negate feedthrough signal and a broad understanding of its origins, there hasn't been a concerted effort to develop a method for accurately determining the values of feedthrough capacitance originating from specific sources. Precisely understanding the contributions of various feedthrough sources is crucial for designing MEMS devices with minimal feedthrough capacitance. In this study, we introduce a systematic approach to assess the contribution of a specific source to the overall value of feedthrough capacitance, $C_{foverall}$.

We have selected an epi-sealed [17] device as our primary platform for experimental work. Ideally, owing to the presence of ground planes above and below the device, feedthrough capacitance should be insignificant when no electrodes are left electrically floating, and the actuation- and sense-electrodes are distant in the device and the connection pads. However, despite these conditions, these devices still exhibit significant feedthrough capacitance. Furthermore, the approach presented in this work can be extended to any MEMS device.

We propose implementing a supplementary capacitance for feedthrough cancellation embedded within the device structure. This approach offers a more compact solution compared to the existing methods. Device-level feedthrough cancellation is expected to enhance noise performance due to a simpler configuration, reduced reliance on external components, and the high performance of single crystal silicon, the material in which the device is fabricated. Additionally, we discuss the impact of partial-electrode actuation/sensing compared to extended-electrode action/sensing on the ratio of the peak resonant signal to the feedthrough signal.

THEORY

To quantify the contribution of feedthrough from various sources, we fabricated an epi-sealed DETF resonator with segmented electrodes, schematic of which is shown in Fig 1. Subsequently, two carrier packages, one with a wire-bonded device affixed on it, and the other without any device, were soldered to a PCB breakout board (Fig 2 & Fig 3).

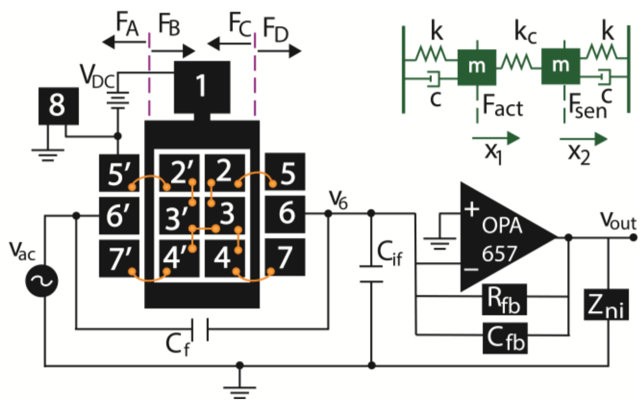

Fig 1: Schematic of the segmented-electrode DETF under test, highlighting forces acting upon it, along with a representation of coupled spring mass equivalent.

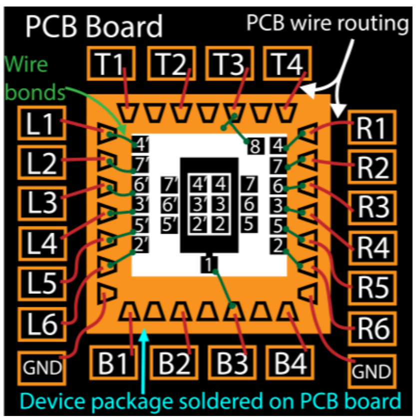

Fig 2: Schematic of the device wire bonded to the carrier package Spectrum LCC02861, which is further mounted on a custom designed PCB. This setup is used for resonance measurement.

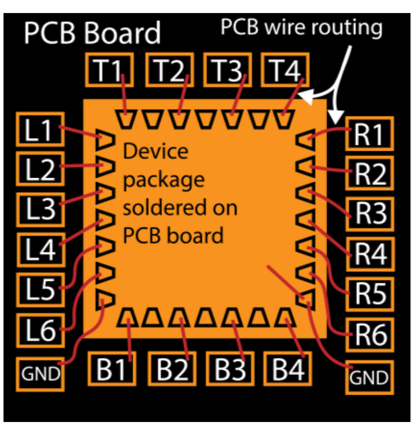

Fig 3: Schematic of empty carrier package Spectrum LCC02861 mounted on a custom designed PCB. This setup is used to quantify the contribution of the PCB + carrier package to the overall feedthrough capacitance.

We identify the sources of feedthrough in an epi-sealed device to be: i) device electrodes, ii) device bondpads, iii) PCB + carrier package footprints, iv) Wirebonds + fringe fields.

To quantify the exact contribution of each of these sources several measurements of the $S21$-parameters between the actuation- and sensing-electrodes were performed using a TIA, at frequencies significantly lower than the first in-plane resonant frequency mode. While measuring the feedthrough capacitance between any two electrodes, we grounded all unused electrodes—otherwise left electrically floating—along with the cap layer and the substrate.

The feedthrough capacitance calculations are outlined in the following equation:

$$V_{out} = -j\omega R_{fb} C_f v_{ac} - j\omega R_{fb} V_{DC} \left(\frac{\epsilon A}{g}\right)\left(\frac{x}{g}\right) \qquad (1)$$

$$C_f = \frac{\left|\frac{v_{out}}{v_{ac}}\right|\Big|_{V_{DC}=0V}}{\omega R_{fb}} \qquad (2)$$

The measurements were performed for the following cases: a) far apart segmented-electrodes and bondpads, b) segmented-electrodes and bondpads in immediate vicinity, c) bondpads apart but adjacent segmented-electrodes, and d) fully-extended-electrodes and bondpads far apart.

The measurements were repeated in absence of the device, with the package still soldered to the PCB (Fig 3) to quantify the contribution of feedthrough capacitance from the PCB + package setup.

EXPERIMENTAL RESULTS

The measurement setup is shown in Fig 4. The S-parameter measurements were carried out using Keysight VNA M9800A.

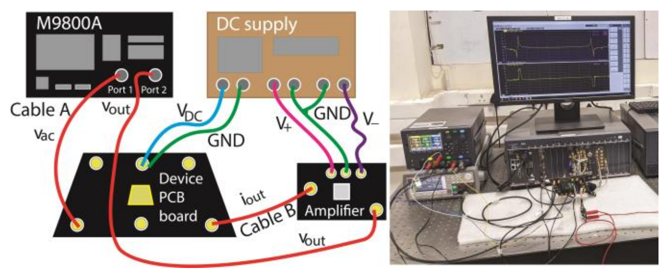

Fig 4: On left is the schematic illustrating the connection setup of the resonance measurement system. On right is the active measurement setup showcasing the characterization of the first two in-plane resonance modes.

To measure feedthrough capacitance between various electrodes, S21 parameters were recorded in frequency range of 9kHz to 90kHz. An illustrative measurement is presented in Fig 5, for the case when electrode 6' was made the actuation electrode and electrode 6 was made the sense-electrode. Remaining electrodes including the resonator were grounded.

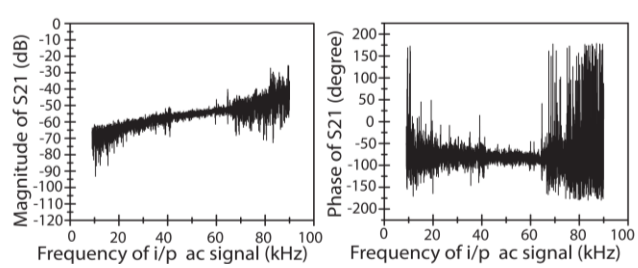

Fig 5: Magnitude and phase of the measured feedthrough signal between L3 & R3 when the device is affixed to the package. This data is used to calculate the feedthrough capacitance C_f.

These measurements were repeated for other sets of actuation and sense electrodes, for the cases when i) device was kept affixed on the carrier package and ii) when the device was removed from the carrier package. The experimental findings and the source of feedthrough in each case are summarized in Table 1.

Table 1: Measured values of feedthrough capacitance (in fF) between various input and output terminal combinations for the setup with and without the device affixed on the package for the measurement cases listed in section 'Theory'.

	(a) C_f between L3 & R3 (in fF)	(b) C_f between R2 & R3 (in fF)	(c) C_f between R5 & R3 (in fF)	(d) C_f between L2, L3, L5 & R2, R3, R5 (in fF)
(1) Without Device	C_{f1} 10.84	C_{f3} 77.43	C_{f5} 12.35	C_{f9} 34.27
(2) With Device	C_{f2} 10.90	C_{f4} 367.23	C_{f6} 54.82	C_{f10} 58.32
Origin of Cf in Device	**PCB** $\boldsymbol{C_{f2} \approx C_{f1}}$	**Proximity of bondpads + electrodes on PCB & device**	**Proximity of electrodes on device**	**PCB** $\boldsymbol{C_{f9} \approx 3C_{f1}}$; $\boldsymbol{C_{f10} \approx C_{f9} +}$ **wirebonds**

The calculation of individual feedthrough contribution of various sources, using measurements from the experiments, is outlined in the following Table 2.

Table 2: Calculated values of various feedthrough contributors using measurements shown in Table 1.

C_α	$C_{PCB\_base} = C_{f1}$	Case a1	10fF
C_β	$C_{electrode\_device} = (C_{f6} - C_{f5})$	Case c2-c1	42fF
C_γ	$C_{electrode\_PCB} = C_{f3}$	Case b1	77fF
C_δ	$C_{device\_bondpad} = (C_{f4} - C_{f3}) - (C_{f6} - C_{f5})$	Case (b2-b1)-(c2-c1)	250fF
C_θ	$C_{extended\_electrode\_PCB} \approx 3C_{f1}$	Case d1	34fF
C_η	$C_{extended\_electrode} = C_{f9} + wirebonds$	Case d2	58fF

It was found that the PCB contributes approximately $C_{PCB\_base} \sim 10fF$ of base capacitance between any two electrodes, while proximity of device-electrodes contributes $C_{electrode\_device}$~42fF. Colocation of these electrodes on PCB further adds $C_{electrode\_PCB}$~20fF, and bondpad colocation results in $C_{device\_bondpad}$~250fF of feedthrough capacitance. Furthermore, in the configuration under study, shorting adjacent electrodes with distant bondpads increases the feedthrough capacitance threefold ($C_{extended\_electrode}$~30fF) due to the three-fold increase in the area of resulting parallel-plate capacitance. It is important to note that this three-fold increase arises from the PCB footprints and not from the device, had these three electrodes been wire-bonded to the same package footprint, feedthrough signal would not have risen. The presented case is shown to elaborate how a configuration choice can determine the fate of the output signal.

Finally, in Fig 6 we show that the feedthrough can be completely negated at the device level by using a drive scheme where $+vac$ is applied on actuation-electrode and $-vac$ is applied to an appropriately chosen dummy-electrode which contributes equal feedthrough signal to the output electrode as the drive-electrode, but does not affect the actuation force on the DETF.

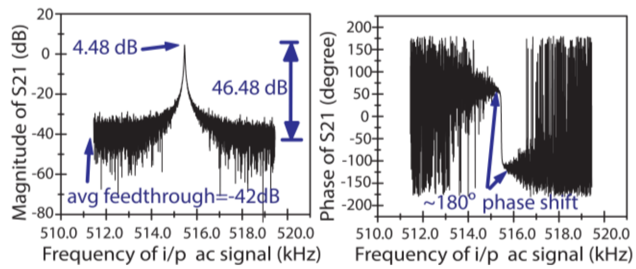

Fig 6: Feedthrough cancellation achieved by supplying $+v_{ac}$ to L3 and $-v_{ac}$ to L6 when output current is sensed at R3. This configuration utilizes an in-situ dummy capacitance to eliminate the impact of C_f.

There is another interesting consequence of using split electrodes. By actuating only the dynamically relevant portion of the beams and sensing from the corresponding split-electrode on the sensed-side contributes to least feedthrough capacitance while achieving maximum actuation. The observed ratio of peak-to-feedthrough signal is much higher when only central electrodes are used as opposed to using all three electrodes on actuation-side and sensed-side, as shown in Fig 7 & Fig 8.

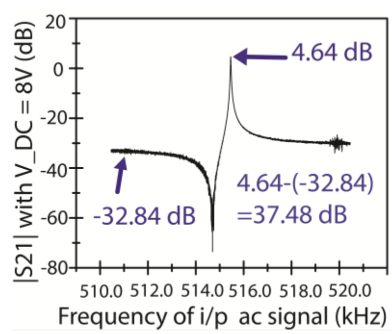

Fig 7: Measured signal showing i) peak height (4.64 dB), ii) feedthrough level (-32.84 dB), iii) ratio of resonance peak and feedthrough level (37.48 dB), when electrode 6' (L3) is set as the input electrode and electrode 6 (R3) is set as the output electrode. Here, $V_{DC} = 8V$ and input power is -35dBm.

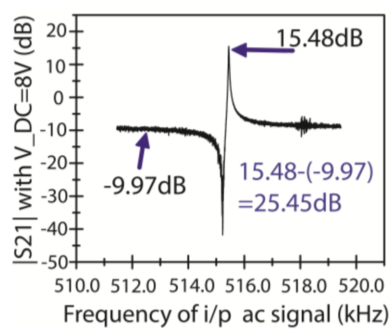

Fig 8: Measured signal showing i) peak height (15.48 dB), ii) feedthrough level (-9.97 dB), iii) ratio of resonance peak and feedthrough level (25.45 dB), when electrode (5',6',7') (L2,L3,L5) is set as the input electrode and electrode (5,6,7) (R2,R3,R5) is set as the output electrode. Here, $V_{DC} = 8V$ and input power is -35dBm

This is because the off-center side electrodes contribute a lot more to the feedthrough signal while contributing much less to the actual displacement signal of the resonator.

MORE DISCUSSION

Similar set of experiments can be done on devices fabricated in other processes. If devices are not encapsulated then measurements can be performed in vacuum chamber to eliminate any stray charges in the system, which lead to time varying feedthrough capacitance in the device under test. Alternatively, as suggested by various research studies, such as [18], the device can be isolated from stray charges present in its external environment using an insulating material.

CONCLUSION

In conclusion, our study delved into quantifying feedthrough contributions from various sources in a capacitive MEMS device through experimentation on epi-sealed devices. We found that, besides proximity of electrodes in the device, arrangement of bondpads in the device, and their layout on the PCB significantly influence feedthrough capacitance. Additionally, by utilizing split electrode configuration, resonant-to-feedthrough signal ratio can be enhanced. We also demonstrate the complete negation of feedthrough signal by fabricating a dummy electrode in the actual device, to which differential drive scheme is employed. Integrating the dummy electrode directly into the device for feedthrough cancellation not only minimizes design complexity but also reduces introduced noise levels in the system. Our findings provide a foundation for further research to optimize device designs and develop innovative solutions for feedthrough mitigation across various fabrication processes.

ACKNOWLEDGEMENTS

We extend our deepest gratitude to Prof. Thomas W. Kenny for his contribution to the development of the epi-seal process. We appreciate his provision of the devices fabricated by his students.

We also express our thanks to the CMTI, Bangalore, for their assistance in providing us with wire-bonded devices.

REFERENCES

[1] S. D. Senturia, *Microsystem Design*. New York, NY: Springer, 2004.

[2] M.-H. Bao, *Analysis and Design Principles of MEMS Devices*. Amsterdam: Elsevier, 2005.

[3] A. Brenes, J. Juillard, F. Vinci Dos Santos, and A. Bonnoit, "Characterization of MEMS resonators via feedthrough de-embedding of harmonic and subharmonic pulsed-mode response," *Sens. Actuators Phys.*, vol. 229, pp. 211–217, Jun. 2015, doi: 10.1016/j.sna.2015.02.032.

[4] M. Riverola, G. Sobreviela, A. Uranga, and N. Barniol, "Intrinsic feedthrough current cancellation in a seesaw CMOS-MEMS resonator for integrated oscillators," in *2016 IEEE International Frequency Control Symposium (IFCS)*, New Orleans, LA, USA: IEEE, May 2016, pp. 1–4. doi: 10.1109/FCS.2016.7546801.

[5] J. E.-Y. Lee and A. A. Seshia, "Direct parameter extraction in feedthrough-embedded capacitive MEMS resonators," *Sens. Actuators Phys.*, vol. 167, no. 2, pp. 237–244, Jun. 2011, doi: 10.1016/j.sna.2011.02.016.

[6] H. Zhang, W. Yuan, Y. Hao, and H. Chang, "Influences of the Feedthrough Capacitance on the Frequency Synchronization of the Weakly Coupled Resonators," *IEEE Sens. J.*, vol. 15, no. 11, pp. 6081–6088, Nov. 2015, doi: 10.1109/JSEN.2015.2453401.

[7] P. Rantakari, J. Kiihamäki, M. Koskenvuori, T. Lamminmäki, and I. Tittonen, "Reducing the Effect of Parasitic Capacitance on MEMS Measurements," in *Transducers '01 Eurosensors XV*, E. Obermeier, Ed., Berlin, Heidelberg: Springer Berlin Heidelberg, 2001, pp. 1528–1531. doi: 10.1007/978-3-642-59497-7_361.

[8] S. A. Bhave, Di Gao, R. Maboudian, and R. T. Howe, "Fully-differential poly-sic lame-mode resonator and checkerboard filter," in *18th IEEE International Conference on Micro Electro Mechanical Systems, 2005. MEMS 2005.*, Miami Beach, FL, USA: IEEE, 2005, pp. 223–226. doi: 10.1109/MEMSYS.2005.1453907.

[9] C.-Y. Wu, Z.-W. Lin, and S.-S. Li, "A Novel Feedthrough Cancellation Technique for Piezoelectric MEMS Resonant Sensors in Ionic Liquid Medium," in *2023 IEEE 36th International Conference on Micro Electro Mechanical Systems (MEMS)*, Munich, Germany: IEEE, Jan. 2023, pp. 905–908. doi: 10.1109/MEMS49605.2023.10052319.

[10] J. E.-Y. Lee and A. A. Seshia, "Parasitic feedthrough cancellation techniques for enhanced electrical characterization of electrostatic microresonators," *Sens. Actuators Phys.*, vol. 156, no. 1, pp. 36–42, Nov. 2009, doi: 10.1016/j.sna.2009.02.005.

[11] Y. Xu and J. E.-Y. Lee, "Single-Device and On-Chip Feedthrough Cancellation for Hybrid MEMS Resonators," *IEEE Trans. Ind. Electron.*, vol. 59, no. 12, pp. 4930–4937, Dec. 2012, doi: 10.1109/TIE.2011.2180274.

[12] J. E.-Y. Lee, Y. Zhu, and A. A. Seshia, "A bulk acoustic mode single-crystal silicon microresonator with a high-quality factor," *J. Micromechanics Microengineering*, vol. 18, no. 6, p. 064001, Jun. 2008, doi: 10.1088/0960-1317/18/6/064001.

[13] P. Jain, G. Gupta, H.-K. Kwon, G. D. Vukasin, and S. A. Chandorkar, "Machine Learning Based Nonlinear Resonator System Identification," in *2024 IEEE 37th International Conference on Micro Electro Mechanical Systems (MEMS)*, Austin, TX, USA: IEEE, Jan. 2024, pp. 541–544. doi: 10.1109/MEMS58180.2024.10439295.

[14] J. E.-Y. Lee, J. Yan, and A. A. Seshia, "Low loss HF band SOI wine glass bulk mode capacitive square-plate resonator," *J. Micromechanics Microengineering*, vol. 19, no. 7, p. 074003, Jul. 2009, doi: 10.1088/0960-1317/19/7/074003.

[15] J. Arcamone, E. Colinet, A. Niel, and E. Ollier, "Efficient capacitive transduction of high-frequency micromechanical resonators by intrinsic cancellation of parasitic feedthrough capacitances," *Appl. Phys. Lett.*, vol. 97, no. 4, p. 043505, Jul. 2010, doi: 10.1063/1.3472217.

[16] J. Giner and K. Ono, "Adaptive feedthrough cancellation in MEMS gyroscopes in reconfigurable IC+FPGA platform," in *2018 IEEE International Symposium on Inertial Sensors and Systems (INERTIAL)*, Moltrasio: IEEE, Mar. 2018, pp. 1–2. doi: 10.1109/ISISS.2018.8358157.

[17] A. Partridge, M. Lutz," U.S. Patent #6928879, Aug 16, 2005.

[18] A. Ali and J. E.-Y. Lee, "Single device on-chip feedthrough cancellation for enhanced electrical characterization of piezoelectric-on-silicon resonators in liquid," *Sens. Actuators Phys.*, vol. 260, pp. 131–138, Jun. 2017, doi: 10.1016/j.sna.2017.04.032.

CONTACT

*Disha Chugh, chughd124@gmail.com

*Saurabh A. Chandorkar, saurabhc@iisc.ac.in